frontiers in Energy Research

TYPE Original Research
PUBLISHED 07 October 2026
DOI 10.3389/fenrg.2026.1946325

Check for updates

OPEN ACCESS

EDITED BY
Chutong Wang,
North China Electric Power University, China

REVIEWED BY
Shuai Geng,
Shandong Jianzhu University, China
Zhaoyuan Wu,
North China Electric Power University, China

*CORRESPONDENCE
Zhongyuan Yan,
emailmy2026@163.com

RECEIVED 23 July 2026
REVISED 21 August 2026
ACCEPTED 31 August 2026
PUBLISHED 07 October 2026

CITATION
Yan Z, Xue W, Zhang Y, Du X and Zheng X (2026) Optimal planning of shared energy storage for wind-solar-thermal distributed energy system clusters based on improved renewable energy forecasting. *Front. Energy Res.* 14:1946325. doi: 10.3389/fenrg.2026.1946325

COPYRIGHT
© 2026 Yan, Xue, Zhang, Du and Zheng. This is an open-access article distributed under the terms of the Creative Commons Attribution License (CC BY). The use, distribution or reproduction in other forums is permitted, provided the original author(s) and the copyright owner(s) are credited and that the original publication in this journal is cited, in accordance with accepted academic practice. No use, distribution or reproduction is permitted which does not comply with these terms.

Optimal planning of shared energy storage for wind-solar-thermal distributed energy system clusters based on improved renewable energy forecasting

Zhongyuan Yan*, Wulei Xue, Yi Zhang, Xinyi Du and Xiande Zheng

Henan Jiuyu Longyuan Energy Service Co., Ltd., Zhengzhou, Henan, China

Aiming at wind-solar intermittency and low coupling between renewable energy forecasting and shared energy storage (SES) planning in wind-solar-thermal distributed energy clusters, this paper proposes a two-stage framework combining high-precision power forecasting and multi-objective SES planning. A VMD-EO-SVM model improves prediction accuracy. A multi-objective planning model minimizes operating costs and maximizes renewable energy accommodation. Case results verify its effectiveness for low-carbon cluster operation.

KEYWORDS
multi-objective planning, power forecasting, shared energy storage, VMD-EO-SVM, wind solar thermal distributed energy system cluster

1 Introduction

1.1 Background

With the advancement of carbon peaking and neutrality targets, wind and solar power have experienced rapid development, accelerating the low-carbon, distributed and flexible transformation of power grids (Li Mengjia et al., 2024). Wind-solar-thermal distributed energy system clusters are widely concerned for boosting local renewable energy consumption and easing grid regulation pressure (Wang et al., 2025). Nevertheless, the inherent volatility and intermittency of wind-solar power degrade system operational efficiency and stability under large-scale integration (Xuejun et al., 2025). Shared energy storage (SES) serves as an effective countermeasure by realizing shared energy regulation, smoothing power fluctuations and curtailment (Li Jinmeng et al., 2024).

Compared with storage systems configured independently for individual distributed energy systems, SES allows multiple generation and consumption entities to use a common storage facility. Differences in renewable generation and load profiles among these entities create partially complementary charging and discharging requirements. Aggregating these requirements through SES can reduce redundant storage capacity and improve the utilization of storage resources. In a wind-solar-thermal distributed energy system cluster, SES can also absorb surplus renewable power from different subsystems and release the stored

energy when additional system flexibility is required. The value of SES therefore lies not only in energy shifting, but also in the coordinated use of storage resources among multiple entities.

From the investment perspective, the shared configuration also allows the capital cost of storage construction to be distributed among participating entities rather than being borne independently by each user. Participants can access the required storage service without constructing a complete storage system for their own use, while the corresponding operating or service costs can be allocated according to the adopted sharing arrangement. This mechanism reduces the financial burden associated with independent storage investment and increases the utilization of installed storage capacity by serving multiple users with heterogeneous demand profiles.

Precise wind-solar power forecasting provides core data for SES planning and operation (Liu and Song, 2025; Jia et al., 2025). In a forecasting-driven planning framework, the predicted renewable power profiles determine the estimated timing and magnitude of power surplus and shortage, which directly affect the required charging and discharging power and the duration of energy shifting. Forecasting errors may therefore propagate to the planning stage and lead to deviations in the estimated power and capacity requirements of SES. Improving forecasting accuracy before storage planning can reduce this source of uncertainty and provide more reliable input for storage configuration. Accordingly, this study integrates renewable power forecasting with SES planning to improve power balance, renewable energy utilization, and the economic operation of wind-solar-thermal distributed energy system clusters.

1.2 Literature review

Renewable power generation suffers strong intermittency, and forecasting methods are categorized into physical, statistical and intelligent types. Physical models rely on meteorological data and NWP (Zhao et al., 2026); statistical approaches adopt ARIMA (Huang, 2026; Yuan et al., 2026; Zhang Yagang et al., 2024), STL (Liu and Zhang, 2024; Zhu et al., 2024; Tong et al., 2026) and regression analysis (Yang et al., 2025); intelligent methods include SVM (Patel et al., 2025; Oruç et al., 2026; Chen et al., 2024), Extreme Learning Machines (ELMs) (Herwan Sulaiman et al., 2025; Bala Duranay, 2023; Zhang Yuhao et al., 2024), LSTM (Dokur et al., 2025), Convolutional Neural Networks (CNNs) (Wen and Xie, 2026) and hybrid models integrating VMD (Peng et al., 2024) and EO (Lin et al., 2025) for better feature extraction.

SES planning is vital for renewable energy consumption in wind-solar-thermal clusters, with existing studies adopting bi-level optimization (Hou et al., 2025), robust optimization (Li et al., 2026), bi-level optimization (Wang et al., 2026), two-stage robust optimization (Kang et al., 2025), cooperative game (Li Cuiping et al., 2024), digital intelligence-driven synergy (Zhou et al., 2025) and other frameworks while considering practical constraints (He and Zhang, 2025). However, renewable power forecasting and storage planning are still commonly treated as separate problems. Forecasting studies mainly focus on reducing prediction errors, whereas SES planning studies generally use predetermined renewable power profiles as model inputs. As a result, the influence of forecasting accuracy on storage configuration has received limited attention. In addition, existing hybrid forecasting methods often focus on either signal decomposition or parameter optimization, while the combined effects of multi-scale decomposition and parameter optimization have not been sufficiently examined. To address these limitations, this study develops a two-stage forecasting and planning framework. VMD is used to extract the multi-scale characteristics of renewable power series, EO is applied to optimize the key parameters of SVM, and the resulting power forecasts are introduced directly into the multi-objective SES planning model. This framework establishes a direct connection between renewable power forecasting and storage configuration and provides a more reliable basis for SES planning under variable renewable generation.

1.3 Highlights

i. A VMD-EO-SVM forecasting method is developed for wind and solar power with strong fluctuations and non-stationary characteristics. VMD first decomposes the original power series into components with different frequency characteristics, thereby reducing the complexity of the forecasting task. EO is then used to optimize the main parameters of SVM for the decomposed components. The component-level forecasts are subsequently reconstructed to obtain the final renewable power forecast. This decomposition-optimization-prediction process improves the ability of the forecasting model to represent renewable power variations at different time scales.

ii. A multi-objective SES planning model is established for wind-solar-thermal distributed energy system clusters using the renewable power forecasts as direct inputs. The model jointly considers system operating cost and renewable energy utilization and determines the rated power and energy capacity of SES under power balance, storage operation, renewable curtailment, and thermal-unit constraints. The proposed framework therefore links improvements in renewable power forecasting with subsequent storage configuration.

iii. The case study verifies the effectiveness of both the forecasting method and the SES planning model. VMD-EO-SVM provides the best overall forecasting performance among the models considered for both wind and solar power. Based on the resulting renewable power forecasts, the optimized SES configuration achieves a renewable energy accommodation rate of 90.3% while maintaining coordinated operation among renewable generation, thermal units, and energy storage. The results demonstrate the practical value of integrating improved renewable power forecasting with SES planning.

The rest of this paper is organized as follows. Section 2 introduces VMD, EO and SVM fundamentals. Section 3 develops the multi-objective SES planning model with objectives and constraints. Section 4 presents the two-stage forecasting-planning coupled framework. Section 5 conducts case validation using measured data. Section 6 draws conclusions.

2 Renewable energy prediction theory and methods

2.1 Multiscale decomposition of volatility–VMD method

Wind power generation is highly random and non-stationary. As an adaptive method for nonlinear non-stationary time series, VMD decomposes historical wind power data into frequency-specific stationary subsequences to reduce complexity, nonlinearity and non-stationarity, with its bandwidth-constrained variational problem mathematically formulated as:

$$\begin{cases} \min\limits_{\{u_k\},\{\omega_k\}} \left\{ \sum\limits_{k=1}^{k} \| \partial_t \left[(\delta(t) + j/\pi t) u_k(t) \right] \exp\left(-j\omega_k t\right) \| \right\} \\ s.t. \sum\limits_{k=1}^{k} u_k = f(t) \end{cases} \tag{1}$$

In the formula, $\delta(t)$ is the Dirac function, that is, the unit impulse function, u_k is the *k-th* modal component, representing each sub-signal obtained by decomposition; ω_k is the center frequency of the *k-th* power modal component; j is the imaginary unit; and $f(t)$ is the original signal to be decomposed. To eliminate the limitations of the above factors, a quadratic penalty operator and a Lagrange multiplier are usually added to transform the minimization problem involved in Equation 2 into an unconstrained optimization problem of Equation 3.

$$\begin{aligned} (\{u_k\},\{\omega_k\},\lambda) = \alpha \sum_{k=1}^{K} \| \partial_t \left[(\delta(t) + j/\pi t) \otimes u_k(t) \right] exp\left(-j\omega_k t\right) \|_2^2 \\ + \| f(t) - \sum_{k=1}^{k} u_k(t) \|_2^2 + \left[\lambda(t), f(t) - \sum_{k=1}^{k} u_k(t) \right] \end{aligned} \tag{2}$$

In this equation, α serves as the quadratic penalty operator. Lambda represents the Lagrange multiplier, and $\otimes$ indicates the convolution operator.

Subsequently, calculate the value of u_k in the frequency domain.

$$\hat{u}_k^{n+1}(\omega) = \left(\hat{f}(\omega) - \sum_{i \neq k} \hat{u}_i^n(\omega) + \frac{\hat{\lambda}^n(\omega)}{2} \right) / \left(1 + 2a\left(\omega - \omega_k^n\right)^2 \right) \tag{3}$$

In the formula, i and n can take arbitrary values, and ω is used to mark the transformation of the signal from the time domain to the frequency domain. $\hat{u}$, $\hat{f}(\omega)$, and $\hat{\lambda}(\omega)$ are the Fourier transformed u, $f(\omega)$ and $\lambda(\omega)$.

Finally, Equations 4, 5 are used to update the relationship between ω_k^{n+1} and λ_k^{n+1}, that is

$$\omega_k^{n+1} = \int_0^{\infty} \omega \left| \hat{u}_k^{n+1}(\omega) \right|^2 d\omega / \int_0^{\infty} \left| \hat{u}_k^{n+1}(\omega) \right|^2 d\omega \tag{4}$$

$$\hat{\lambda}^{n+1}(\omega) \leftarrow \hat{\lambda}^n(\omega) + \tau \left[\hat{f}(\omega) - \sum k\hat{u}_k^{n+1}(\omega) \right] \tag{5}$$

In the formula, τ is the step size parameter for updating the Lagrange multiplier, which will have an impact on the convergence speed and stability of the iteration.

The iteration process is based on the preset noise discrimination accuracy δ. When this accuracy is reached, the iteration is stopped and the operation results are output.

$$\sum k \| \hat{u}_k^{n+1} - \hat{u}_k^n \|_2^2 / \| \hat{u}_k^n \|_2^2 < \varepsilon$$

In the equation, ε represents the convergence progress.

Ultimately, the original power sequence will be decomposed into k narrow-band intrinsic mode functions (IMFs). Each IMF has a different center frequency ω_k in the frequency domain, representing different characteristics of the original signal.

2.2 Equilibrium state measurement of volume–EO method

Benefiting from physical-mechanism-driven search, EO features strong global exploration and rapid convergence by seeking system equilibrium with balanced mass exchange and generation. Its mathematical implementation consists of three main steps.

Step 1: Population particle initialization

The initial concentrations are constructed based on the number of particles and dimensions with uniform random initialization in the search space, as follows:

$$\vec{C}_i^0 = \vec{C}_{\min} + \vec{r}_i \left(\vec{C}_{\max} - \vec{C}_{\min} \right), i = 1, 2 \ldots, N$$

Step 2: Construct the equilibrium pool and select the candidate solution

Before equilibrium in early iterations, the four optimal-fitness particles and their average serve as candidate solutions to determine particle search modes and build an equilibrium pool.

$$\vec{C}_{eq,pool} = \left\{ \vec{C}_{eq(1)}, \vec{C}_{eq(2)}, \vec{C}_{eq(3)}, \vec{C}_{eq(4)}, \vec{C}_{eq(ave)} \right\}$$

Step 3: Exponential term (F)

In order to balance the global search and local search of the algorithm and ensure the convergence of the algorithm, the index is set as follows:

$$\vec{F} = a_1 sign(\vec{r} - 0.5) \left[e^{-\vec{\lambda} t} - 1 \right]$$

where $= 1 - \left(\frac{Iter}{Max_iter} \right)^{a_2 \frac{Iter}{Max_iter}}$; a_1 and a_2 are constant; *Iter* and $Max_i ter$ are the number of current iterations and the maximum number of iterations, respectively; $\vec{\lambda}$ is a random vector between [0,1] whose dimension is the same as the dimension of the optimized space; $sign(\vec{r} - 0.5)$ represents the function used to control the direction of exploration and development;

Step 4: Generation rate (G)

To enhance the local optimization capability of the algorithm, the generation rate is designed as follows:

$$\vec{G} = \vec{G}_0 e^{-\vec{\lambda}(t - t_0)} = \vec{G}_0 \vec{F}$$

$$\vec{G}_0 = G\vec{C}P \left(\vec{G}_{eq} - \vec{\lambda}\vec{C} \right)$$

$$G\vec{C}P = \begin{cases} 0.5 r_1 r_2 \geq GP \\ 0 r_2 < GP \end{cases}$$

where $\vec{G}$ is a randomly selected solution from the equilibrium pool; $G\vec{C}P$ is the control parameter of generation rate G, when GP = 0.5, the algorithm achieves balance between global optimization

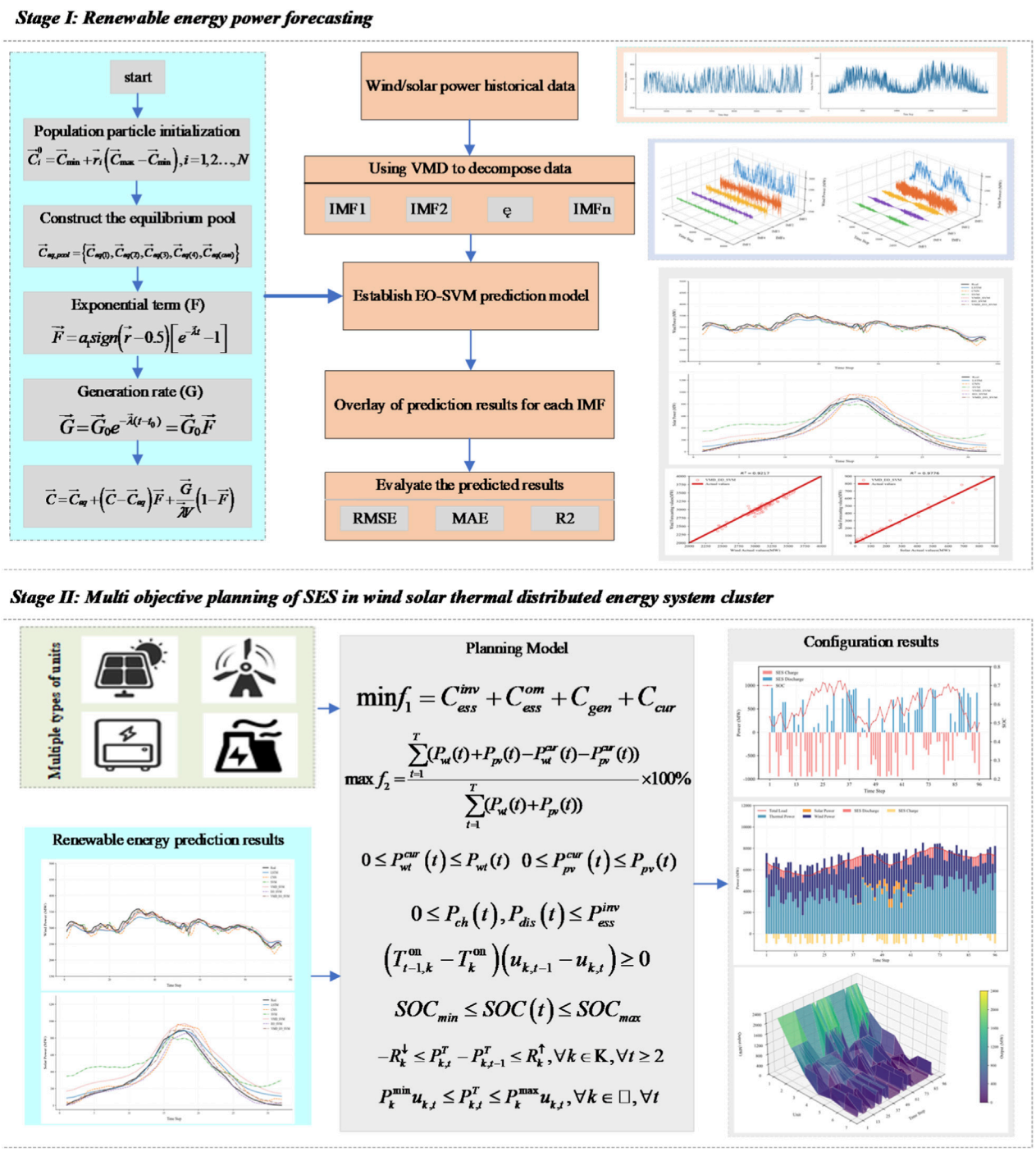

FIGURE 1
The overall framework.

and local optimization. To sum up, the final update formula of EO is as follows:

$$\vec{C} = \vec{C}_{eq} + \left(\vec{C} - \vec{C}_{eq}\right)\vec{F} + \frac{\vec{G}}{\vec{\lambda} V}\left(1 - \vec{F}\right)$$

$\vec{C}_{eq}$ represents the concentration of guide particles selected from the equilibrium pool. $\left(\vec{C} - \vec{C}_{eq}\right)\vec{F}$ is added to find the optimal solution in the global search space by using the concentration difference between sample particle $\vec{C}$ and equilibrium particle $\vec{C}_{eq}$. Through $\vec{F}$, the EO can achieve a reasonable balance between exploration and development. Here, $\frac{\vec{G}}{\vec{\lambda} V}\left(1 - \vec{F}\right)$ produces a small change in concentration through the formation rate $\vec{G}$, which makes the result more accurate.

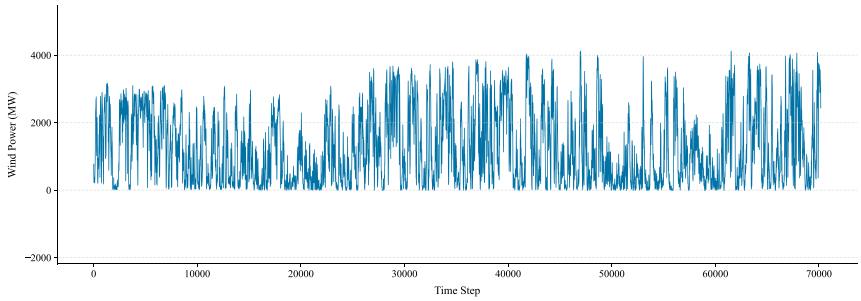

FIGURE 2
Wind power time series.

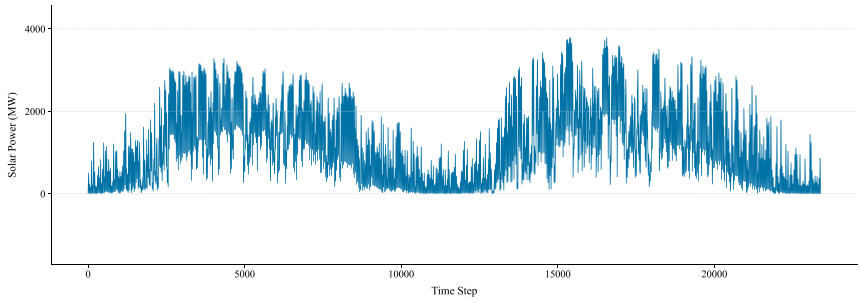

FIGURE 3
Solar power time series.

TABLE 1 The main operational parameters of the thermal power units.

Number	$P^{T,\max}$	$P^{T,\min}$	a	b	c	T^{on}	T^{off}	C^{hot}	C^{cold}	$R^{\uparrow}$	$R_k^{\downarrow}$
1	130	20	0.00200	16.60	700	5	5	550	1,100	130	130
2	130	20	0.00211	16.50	680	5	5	560	1,120	130	130
3	85	25	0.00790	22.74	480	3	3	260	520	80	80
4	80	20	0.00712	22.26	370	3	3	170	340	80	80
5	55	10	0.00413	25.92	660	1	1	30	60	55	55
6	55	10	0.00222	27.27	665	1	1	30	60	55	55
7	55	10	0.00173	27.29	670	1	1	30	60	55	55

TABLE 2 Energy storage system parameters.

Parameters	Value	Unit
Unit capacity cost	1.5×10^6	YUAN/MW
Unit power cost	2×10^6	YUAN/MW
Charging/Discharging efficiency	0.95	—
Unit O&M cost	0.025	YUAN/kWh
SOC upper bound	0.9	—
SOC lower bound	0.1	—
Initial SOC	0.5	—

2.3 Power output prediction–SVM method

In SVM modeling, each input sample x_i in a low-dimensional space is first mapped into a higher-dimensional feature space through a nonlinear mapping function $\phi(x)$. Subsequently, a linear regression function is constructed in this high-dimensional space, which can be expressed as:

$$f(x) = \omega \cdot \phi(x) + bx \in \mathbb{R}^d, b \in \mathbb{R}$$

To transform the regression problem into a tractable optimization task, the structural risk minimization principle is adopted. Specifically, a tolerance parameter ε is introduced to define

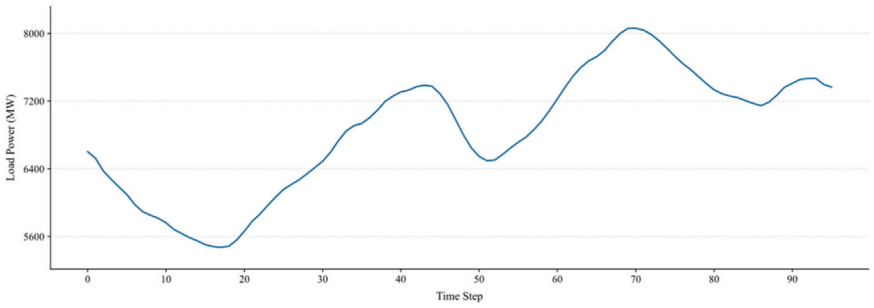

FIGURE 4
Load curve.

an insensitive loss zone, within which errors are not penalized. To account for samples outside this zone, two slack variables ξ_i and ξ_i^* are added to relax the constraints. The resulting optimization problem is formulated as

$$\min_{\omega,b,\xi,\xi^*} \frac{1}{2} \| \omega \|^2 + C\sum_{i=1}^{n} (\xi_i + \xi_i^*)$$

Subject to the following constraints:

$$\begin{cases} y_i - \omega \cdot x_i - b \le \vartheta + \xi_i \\ \omega \cdot x_i + b - y_i \le \vartheta + \xi_i^* \\ \xi_i \ge 0 \\ \xi_i^* \ge 0 \end{cases} \quad i = 1, 2, \cdots, n$$

To solve this constrained optimization problem, the Lagrange multiplier method is employed. By constructing the Lagrangian function and applying the duality theorem, the original problem is transformed into a dual optimization problem involving the maximization of the following objective function:

$$max \left\{ \begin{array}{l} -\frac{1}{2}\sum_{i,j=1}^{n} (\alpha_i - \alpha_i^*)(\alpha_j - \alpha_j^*) K(x_i, x_j) \\ +\sum_{i=1}^{n} (\alpha_i - \alpha_i^*) y_i - \vartheta \sum_{i=1}^{n} (\alpha_i + \alpha_i^*) \end{array} \right\}$$
$$\text{s.t.} \sum_{i=1}^{n} (\alpha_i - \alpha_i^*) = 0 \quad \alpha_i, \alpha_i^* \in [0, C]$$

where α_i, α_i^* are the Lagrange multipliers associated with each constraint, and $K(x_i, x_j) = \phi(x_i) \cdot \phi(x_j)$ denotes the kernel function used to compute the inner product in the high-dimensional space without explicitly performing the nonlinear mapping. Based on the solution of the dual problem, the final regression function can be ex pressed as

$$f(x) = \sum_{i=1}^{n} (\alpha_i - \alpha_i^*) K(x_i, x) + b$$

Among various kernel functions, the radial basis function (RBF) is often considered ideal for its wide convergence region and high resolution. Therefore, the RBF is selected as the kernel function in this study, defined as

$$K(x, x_j) = \exp\left(-\frac{\| x - x_j \|^2}{2v^2} \right)$$

where v controls the width of the RBF kernel.

Based on the above methods, the proposed forecasting procedure connects VMD, EO, and SVM in sequence. The original renewable power series is first decomposed by VMD into several frequency-specific components. EO then searches for suitable values of C and γ for the SVM prediction model. The optimized SVM is applied to each decomposed component, and the resulting component-level forecasts are reconstructed to obtain the final wind or solar power forecast. This procedure allows signal decomposition and parameter optimization to be incorporated into the same forecasting process.

3 Multi-objective planning model of SES in wind-solar-thermal distributed energy system clusters

The SES planning stage uses the wind and solar power profiles obtained from the forecasting stage as time-varying inputs. These profiles describe the expected timing and magnitude of renewable power surplus and shortage and are therefore directly related to power balance, renewable curtailment, and storage operation. Higher forecasting accuracy can reduce the difference between the renewable power assumed during planning and the expected operating conditions. This provides a more reliable basis for determining the rated power, energy capacity, and charging and discharging requirements of SES.

The planning model considers two objectives: minimizing the total system cost and maximizing renewable energy utilization. The main planning variables are the rated power and energy capacity of SES, while the operational variables include charging and discharging power, thermal-unit output, and renewable energy curtailment over the scheduling horizon. For each storage configuration, system operation must satisfy the power balance constraint, renewable curtailment limits, SOC and charging and discharging constraints, and the operating constraints of thermal units. Increasing the size of SES can provide greater flexibility for absorbing renewable power and supporting the system during periods of power shortage. However, a larger storage system also increases investment and operation costs. The planning model therefore determines a storage configuration that balances economic performance

10.3389/fenrg.2026.1946325

TABLE 3 Parameter settings of the forecasting models.

Model	Parameter	Value
LSTM	Optimizer	Adam
	Initial learning rate	0.001
	Loss function	MSE
	Number of training epochs	30
	Batch size	32
	Input tensor shape	(48,1)
CNN	Conv1D filters	64
	Kernel size	2
	Activation function	ReLU
	Max pooling window size	2
	Dense hidden layer units	50
	Activation of dense layer	ReLU
	Output layer units	1
	Optimizer	Adam
	Initial learning rate	0.001
	Loss function	MSE
	Number of training epochs	50
	Batch size	32
	Input tensor shape	(48,1)
VMD	Quadratic penalty factor	500
	Dual ascent time step	0
	Number of intrinsic mode functions	5
	DC component flag	0
	Center frequency initialization mode	1
	Convergence tolerance	1×10^{-7}
EO-SVM	Population size	20
	Maximum iterations	30
	Search range of C	[1, 800]
	Search range of γ	[0.005, 50]
VMD-EO-SVM	Population size	15
	Maximum iterations	20
	Search range of C	[1, 800]
	Search range of γ	[0.005, 50]

and renewable energy utilization under the specified system conditions.

3.1 Objective function

To support the economic and stable operation of wind-solar-thermal distributed energy system clusters, a multi-objective SES planning model is established with the objectives of minimizing the total system cost and maximizing renewable energy utilization.

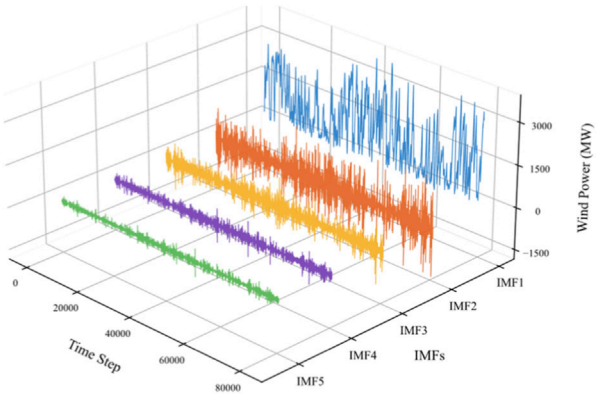

FIGURE 5
Wind power decomposition results.

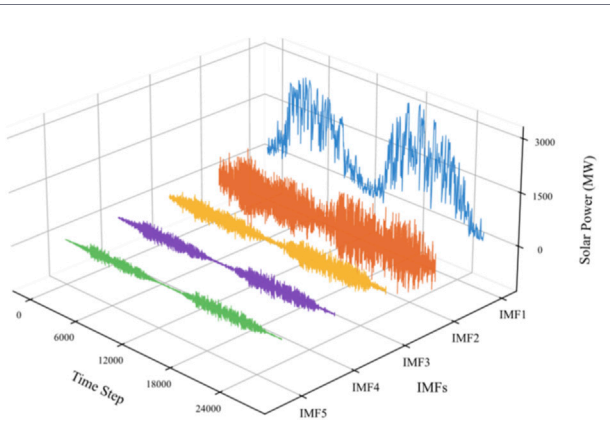

FIGURE 6
Solar power decomposition results.

i. Minimization of Total Cost
The total costs include SES investment costs, operation and maintenance costs, thermal power, thermal power generation costs, and penalties for renewable energy curtailment:

$$\min f_1 = C_{ess}^{inv} + C_{ess}^{om} + C_{gen} + C_{cur}$$

where:

$$C_{ess}^{inv} = \lambda_{ess}^{P} P_{ess}^{inv} + \lambda_{ess}^{E} E_{ess}^{inv}$$

$$C_{ess}^{om} = \sum_{t=1}^{T} \lambda_{ess}^{om} \left(P_{ess}^{ch}(t) + P_{ess}^{dch}(t) \right)$$

$$C_{k,t}^{\text{gen}} = a_k \left(P_{k,t}^{T} \right)^2 + b_k P_{k,t}^{T} + c_k$$

$$C_{k,t}^{\text{su}} = y_{k,t} \left[C_k^{\text{hot}} \cdot \mathbb{I}\left(T_{k,t}^{\text{off}} | T_k^{\text{th}} \right) + C_k^{\text{cold}} \cdot \mathbb{I}\left(T_{k,t}^{\text{off}} | T_k^{\text{th}} \right) \right]$$

$$C^{\text{gen}} = \sum_{t=1}^{T} \sum_{k \in \mathcal{K}} \left(C_{k,t}^{\text{gen}} + C_{k,t}^{\text{su}} \right)$$

$$C_{cur} = \sum_{t=1}^{T} \lambda_{cur} \left(P_{wt}^{cur}(t) + P_{pv}^{cur}(t) \right)$$

TABLE 4 Comparison of prediction evaluation metrics.

Power source	Model	RMSE	MAE	R^2	RMSE reduction (%)
Solar power	LSTM	69.59484	54.98463	0.940152	38.79
	CNN	94.8588	76.39507	0.888813	55.09
	SVM	195.2069	163.2274	0.529144	78.18
	VMD_SVM	134.5773	127.0446	0.77621	68.34
	EO_SVM	56.08481	39.20254	0.961132	24.04
	VMD_EO_SVM	42.60187	34.39801	0.977574	--
Wind power	LSTM	115.7697	95.72683	0.796721	37.95
	CNN	145.6358	111.2154	0.678308	50.68
	SVM	91.30005	71.8252	0.873571	21.32
	VMD_SVM	95.27666	76.86092	0.862318	24.61
	EO_SVM	84.84396	69.06821	0.89082	15.33
	VMD_EO_SVM	71.83382	54.55224	0.921736	--

The SES investment cost in the objective function is expressed on an equivalent daily basis rather than as the total initial capital expenditure. The initial investment associated with the rated power and energy capacity of SES is allocated over the service life of the storage system and then converted to the 24-h scheduling horizon considered in this study. Therefore, the SES investment cost reported in the planning results represents the daily equivalent investment cost corresponding to the optimized storage configuration.

ii. Maximization of renewable energy utilization rate

The renewable energy utilization ratio is defined as the proportion of actually utilized renewable energy to the total available renewable energy:

$$\max f_2 = \frac{\sum_{t=1}^{T}\left(P_{wt}(t)+P_{pv}(t)-P_{wt}^{cur}(t)-P_{pv}^{cur}(t)\right)}{\sum_{t=1}^{T}\left(P_{wt}(t)+P_{pv}(t)\right)} \times 100\%$$

where: $P_{wt}(t)$ and $P_{pv}(t)$ denote the forecasted wind and photovoltaic power during time period t.

3.2 Constraint

i. Power Balance Constraint

Ensures the supply-demand balance at each time step:

$$\sum_{k\in\mathcal{K}} P_k^T(t) + P_{wt}(t) + P_{pv}(t) - P_{wt}^{cur}(t) - P_{pv}^{cur}(t) + P_{ess}^{dch}(t) - P_{ess}^{ch}(t) + P_{grid}(t) = P_{load}(t)$$

ii. Curtailment Constraints

Wind and solar curtailment is less than the predicted power:

$$0 \le P_{wt}^{cur}(t) \le P_{wt}(t)$$

$$0 \le P_{pv}^{cur}(t) \le P_{pv}(t)$$

iii. Energy Storage Constraints

These constraints describe the operational characteristics of the energy storage system.

$$SOC(t+1) = SOC(t) + \frac{\eta_{ch}P_{ess}^{ch}(t) - P_{ess}^{dch}(t)/\eta_{dch}}{E_{ess}^{inv}}$$

$$0 \le P_{ch}(t), P_{dis}(t) \le P_{ess}^{inv}$$

$$P_{ch}(t) \perp P_{dis}(t)$$

$$SOC_{min} \le SOC(t) \le SOC_{max}$$

iv. Operational Constraints of Thermal Power Units

$$P_k^{\min} u_{k,t} \le P_{k,t}^T \le P_k^{\max} u_{k,t}, \forall k \in \mathcal{K}, \forall t$$

$$-R_k^{\downarrow} \le P_{k,t}^T - P_{k,t-1}^T \le R_k^{\uparrow}, \forall k \in \mathcal{K}, \forall t \ge 2$$

$$\left(T_{t-1,k}^{\text{on}} - T_k^{\text{on}}\right)\left(u_{k,t-1} - u_{k,t}\right) \ge 0$$

$$\left(T_{t-1,k}^{\text{off}} - T_k^{\text{off}}\right)\left(u_{k,t} - u_{k,t-1}\right) \ge 0$$

$$y_{k,t} \ge u_{k,t} - u_{k,t-1}, \forall k \in \mathcal{K}, \forall t \ge 2$$

$$y_{k,t} \in \{0,1\}, u_{k,t} \in \{0,1\}$$

4 Framework

The overall research framework consists of two consecutive stages: renewable power forecasting and multi-objective SES planning for wind-solar-thermal distributed energy system clusters. The complete research procedure is illustrated in Figure 1.

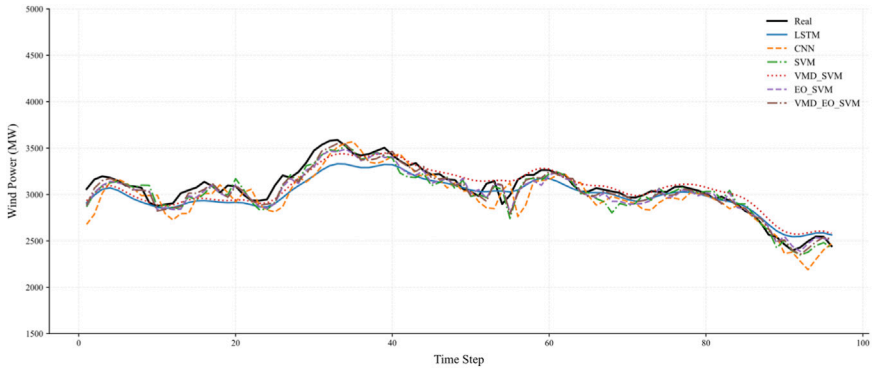

FIGURE 7
Comparison of wind power forecasting curves.

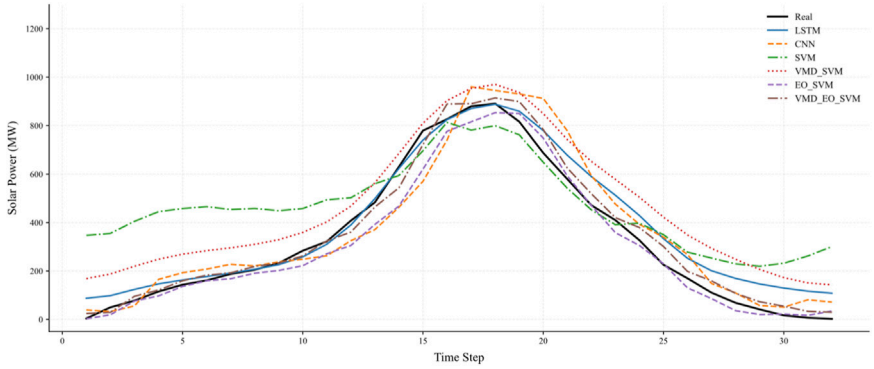

FIGURE 8
Comparison of solar power forecasting curves.

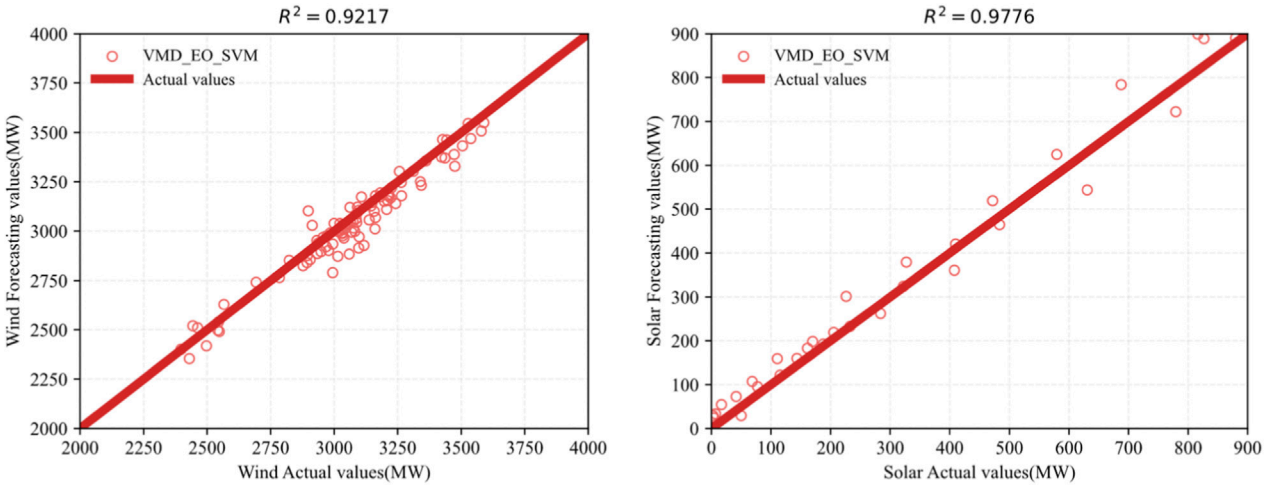

FIGURE 9
Parity plots of predicted values.

TABLE 5 Key indicators of the SES multi-objective planning result.

$\sum_{t=1}^{T}\sum_{k\in K} C_{k,t}^{gen}$ (YUAN)	$\sum_{t=1}^{T}\sum_{k\in K} C_{k,t}^{su}$ (YUAN)	C_{ess}^{om} (YUAN)	C_{cur} (YUAN)	C_{ess}^{inv} (YUAN)	P_{ess}^{inv} (MW)	E_{ess}^{inv} (MWh)	f_1 (YUAN)	f_2 (%)
64,311,393	41,720	352,507	366,611	1,884,453	947	5,615	66,956,684	90.3

5 Case study

5.1 Data description

This study adopts 15-min-interval measured wind-solar power data from Belgium (2020–2021) with high temporal resolution to capture short-term generation fluctuations. Missing values are imputed and outliers eliminated in preprocessing to guarantee data quality. Given the diurnal characteristic of photovoltaic power (negligible output outside 8:45–16:30), only data within this window are used for modeling to avoid redundancy and improve efficiency. Processed wind-solar time series are shown in Figures 2 and 3.

The main operational parameters of the thermal power units in the distributed energy system are listed in Table 1, while the energy storage system is treated as a configuration object, and its main parameters are given in Table 2.

The unit power and capacity costs in Table 2 represent the initial capital investment parameters of SES. These parameters are converted to equivalent daily investment costs according to the service life of the storage system when calculating the objective function.

The load data used in this study corresponds to a typical daily load profile measured in a region of Belgium, with a time resolution of 15 min, covering the electricity demand variations over a 24-h period, as shown in Figure 4. This dataset is used to represent the load characteristics under typical operating conditions.

To improve the reproducibility of the forecasting experiments, the main parameter settings of VMD, EO, LSTM, and CNN are provided in Table 3. For VMD, the original renewable power series is decomposed into five IMFs using a quadratic penalty factor of 500 and a convergence tolerance of 1×10^{-7}. For EO, the population sizes are set to 20 for EO-SVM and 15 for VMD-EO-SVM, while the corresponding maximum numbers of iterations are 30 and 20. The search ranges of C and γ are set to [1, 800] and [0.005, 50], respectively, for both models. The benchmark LSTM and CNN models use the same input tensor shape of (48, 1) and are trained using the Adam optimizer, an initial learning rate of 0.001, and the MSE loss function. Detailed parameter settings are summarized in Table 3.

5.2 Prediction results analysis

5.2.1 VMD decomposition results

To characterize the multi-scale features of wind and photovoltaic power series, the VMD method is employed to decompose the original time series into a set of IMFs with limited bandwidth. The decomposition results are presented in Figures 5 and 6, respectively.

As illustrated in Figures 5 and 6, wind and solar power series are decomposed into frequency-stratified modal components: high-frequency parts capture short-term fluctuations, whereas medium-/low-frequency counterparts reflect the overall smooth temporal trends with favorable multi-timescale separability.

5.2.2 Prediction performance analysis

To quantify wind-solar power forecasting performance, RMSE, MAE and R^2 are used as metrics (Table 4). The proposed VMD-EO-SVM outperforms all counterparts: for solar power, it attains RMSE = 42.60, MAE = 34.40 and R^2 = 0.9776, greatly lowering prediction errors and enhancing fitting consistency relative to basic SVM, EO-SVM and VMD-SVM; for wind power, it achieves RMSE = 71.83, MAE = 54.55 and R^2 = 0.9217, outperforming SVM and CNN with reduced errors and improved goodness-of-fit. Overall, deep learning models (LSTM, CNN) perform poorly in error indices, while conventional SVM suffers from limited overall accuracy despite partial stability.

The results of SVM, VMD-SVM, EO-SVM, and VMD-EO-SVM also provide a component-level comparison of the proposed forecasting framework. For solar power, the RMSE decreases from 195.21 for SVM to 56.08 for EO-SVM, indicating that parameter optimization substantially improves the prediction performance of SVM. When VMD is further combined with EO-SVM, the RMSE decreases to 42.60, which represents a reduction of 24.04% relative to EO-SVM. A similar pattern is observed for wind power. The RMSE decreases from 91.30 for SVM to 84.84 for EO-SVM and further to 71.83 for VMD-EO-SVM, corresponding to an additional reduction of 15.33% relative to EO-SVM.

The results also show that the contribution of VMD depends on its integration with the forecasting model. For wind power, VMD-SVM does not outperform the original SVM in terms of RMSE, which indicates that signal decomposition alone does not necessarily improve prediction accuracy. In contrast, VMD-EO-SVM achieves the lowest RMSE and MAE and the highest R^2 for both wind and solar power. This result suggests that VMD and EO perform complementary functions. VMD reduces the complexity of the original power series by separating variations at different frequency scales, while EO improves the parameter configuration of SVM. Their combined use provides more stable forecasting performance than either component used separately.

To provide a more direct comparison with the benchmark models, Table 4 also reports the percentage reduction in RMSE achieved by VMD-EO-SVM relative to each comparison model. For solar power, the RMSE is reduced by 38.79%, 55.09%, 78.18%, 68.34%, and 24.04% relative to LSTM, CNN, SVM, VMD-SVM, and EO-SVM, respectively. For wind power, the corresponding reductions are 37.95%, 50.68%, 21.32%, 24.61%, and

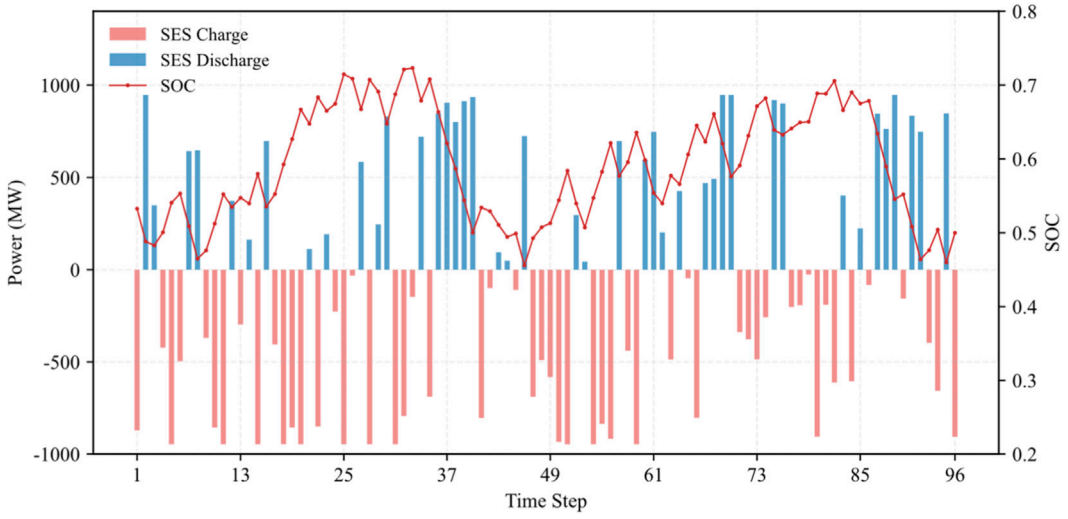

FIGURE 10
Charge/discharge power of SES.

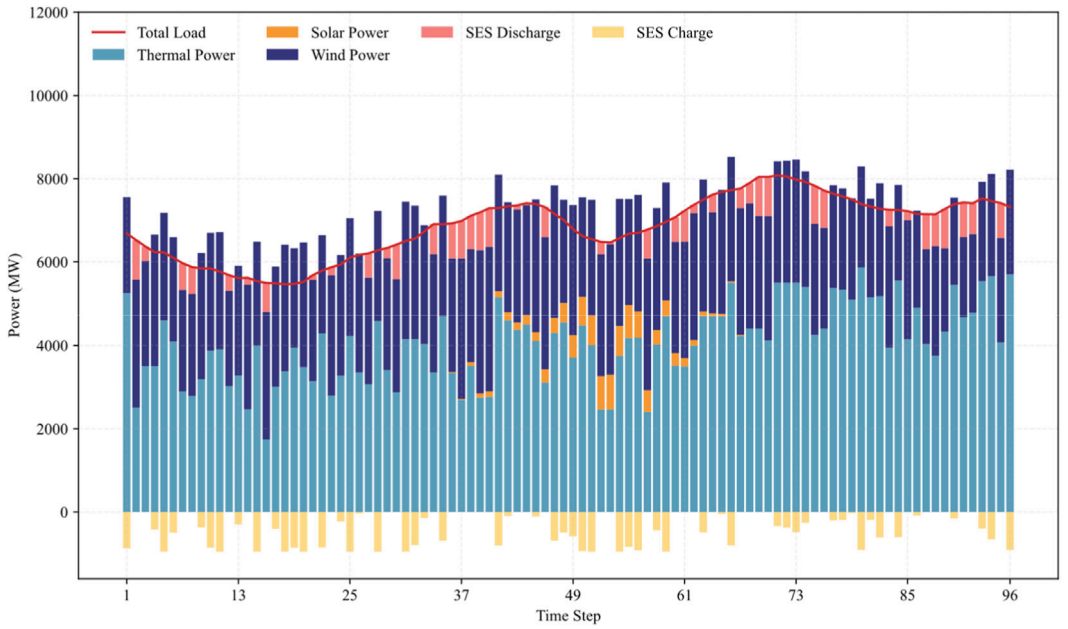

FIGURE 11
Real-time power balance.

15.33%. These results provide a more direct quantitative comparison of the forecasting improvement achieved by VMD-EO-SVM.

As shown in Figure 7, wind power forecasting curves demonstrate that the proposed VMD-EO-SVM closely tracks actual power values across the whole period, especially under strong fluctuations, whereas other models show obvious deviations.

LSTM and CNN underestimate peaks and smooth sharp variations, losing local details; conventional SVM and VMD-SVM track trends poorly at abrupt transitions. By contrast, VMD-EO-SVM maintains superior amplitude-trend consistency, especially at peaks and valleys. Consistent with solar forecasting results in Figure 8, its prediction closely matches actual output throughout daylight hours and better approximates peak generation, while other models suffer from lag or overestimation.

Moreover, parity plots further verify model fitting performance (Figure 9). Wind power predictions of VMD-EO-SVM cluster closely around the diagonal with R^2 = 0.9217,

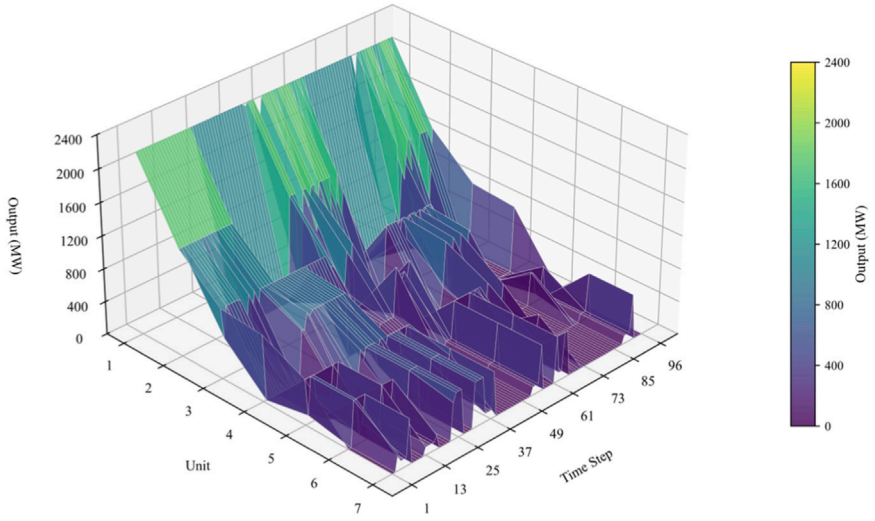

FIGURE 12
Unit output distribution.

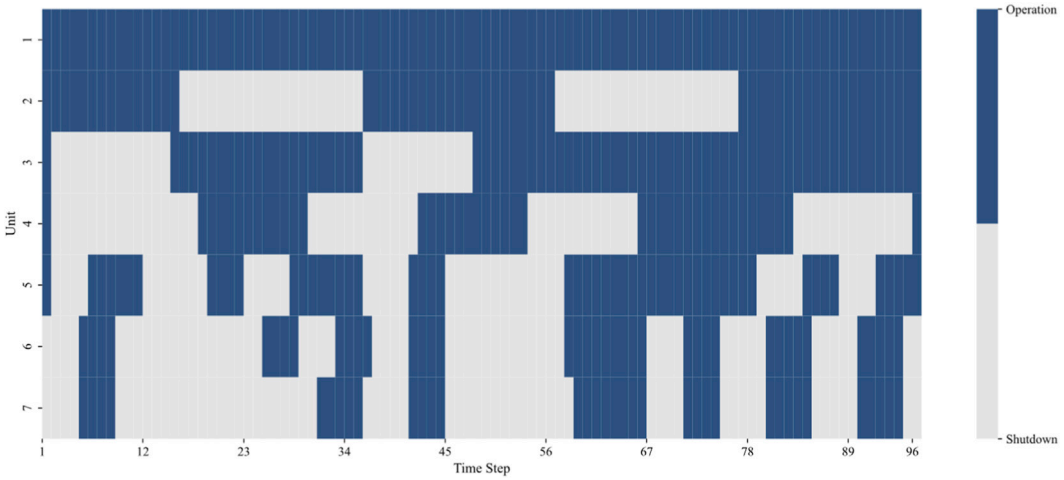

FIGURE 13
Unit start/stop heatmap.

while solar power points are more tightly distributed along the diagonal and achieve R^2 = 0.9776, demonstrating superior fitting accuracy.

5.3 Configuration results analysis

5.3.1 SES configuration and operational characteristics

Table 5 summarizes the main results of the multi-objective SES planning model. Under the system conditions considered in this study, the optimized rated power and energy capacity of SES are 947 MW and 5,615 MWh, respectively. The corresponding energy-to-power ratio is approximately 5.93 h. This duration indicates that SES is required not only to smooth short-term power fluctuations but also to shift energy across several hours. The rated power determines the ability of the storage system to respond to relatively large short-term differences between renewable generation and system demand, while the energy capacity determines the amount of renewable energy that can be transferred from surplus periods to periods of insufficient generation or high load.

The optimized configuration also reflects the trade-off between renewable energy utilization and storage cost. Increasing the rated power and energy capacity can improve the ability of the system to absorb surplus renewable generation and reduce the regulation requirements of thermal units. However, an excessively large storage system would increase investment and operation costs. With the optimized configuration of 947 MW and 5,615 MWh, the renewable energy accommodation

rate reaches 90.3%, while the total system cost is 66,956,684 CNY. The operating results in Figure 10 further support the rationality of this configuration. SES mainly charges during periods of renewable power surplus and discharges when renewable generation is insufficient or load demand is relatively high, while SOC remains within the specified operating range. These results indicate that the storage configuration is determined by both the magnitude and temporal distribution of the imbalance between renewable generation and system demand.

Figure 10 shows SES operational features: it follows low-charge and high-discharge operation with charge-discharge mutual exclusion, and its SOC remains within the safe 0.1–0.9 range without overcharge or overdischarge. SES charges to absorb excess wind-PV power during high-output periods to reduce curtailment, and discharges heavily at peak loads to supplement power supply and ease thermal power peaking pressure.

5.3.2 System power balance analysis

Figure 11 shows the 96-period power distribution of the wind-solar-thermal system with SES, confirming real-time power balance at each time step.

Wind and solar power exhibit obvious temporal complementarity, providing stable renewable supply with daytime solar generation and nighttime wind output. Thermal power acts as the base source to dynamically regulate power for system reliability, while SES optimizes power balance by storing excess renewable power in low-load periods and releasing it at peak loads to ease thermal peaking pressure. Such multi-source coordination mitigates renewable intermittency and realizes efficient power balance throughout the scheduling cycle.

5.3.3 Thermal power unit output characteristics

Figures 12 and 13 depict the operation of seven thermal power units. Units 1–2 operate stably as base-load units, whereas Units 3–7 act as peaking units with dynamic output regulation. Peaking units are shut down during high renewable generation to cut coal use, leading to low startup-shutdown costs (41,720 CNY). All units satisfy ramp-rate and minimum on/off-time constraints for stable power adjustment.

6 Conclusion

This study develops a VMD-EO-SVM-based high-precision wind-solar power forecasting approach and a multi-objective SES planning model for wind-solar-thermal distributed energy clusters. Combining variational mode decomposition with equilibrium optimizer tuning, VMD-EO-SVM well captures non-stationary and nonlinear characteristics of wind-solar series, outperforming SVM, LSTM, CNN and other benchmarks with solar metrics (RMSE = 42.60, MAE = 34.40, R^2 = 0.9776) and wind metrics (RMSE = 71.83, MAE = 54.55, R^2 = 0.9217).

The SES planning model minimizes operational costs and maximizes renewable accommodation, jointly optimizing SES sizing and operation strategies. Case studies yield an SES rated power of 947 MW and capacity of 5,615 MWh, with total system cost of 66,956,684 CNY and a 90.3% renewable accommodation rate, supporting real-time power balance and hierarchical thermal unit dispatch.

From the perspective of resource sharing, SES provides a common source of operational flexibility for the distributed energy system cluster. Different wind, solar, load, and thermal regulation requirements can be coordinated through the same storage facility. This shared use can improve the utilization of storage resources and reduce redundant storage capacity that may result from independent configuration for individual subsystems. The planning results therefore reflect not only the energy-shifting function of storage but also the value of coordinated storage use among multiple entities. The shared configuration also provides a practical basis for distributing storage investment among multiple participants, thereby reducing the capital burden on individual users while improving the utilization of the common storage resource.

The results also provide practical implications for the planning of renewable-energy-based distributed energy system clusters. Renewable power forecasting and storage configuration should be considered within a coordinated planning process because forecasting errors can affect the estimated storage requirements. Improving the quality of renewable power forecasts can therefore support more reliable SES configuration. For the practical application of SES, clear mechanisms are also required for capacity allocation, charging and discharging priority, cost sharing, and benefit distribution among participating entities. These arrangements can improve the utilization of shared storage resources and reduce unnecessary duplication of independently configured storage. Future demonstration projects may further evaluate forecasting accuracy, renewable energy accommodation, storage utilization, and system cost within a common assessment framework to support integrated planning and operation.

A limitation of the present study is that the forecasting model mainly uses historical power data and does not explicitly include meteorological variables. Historical wind and photovoltaic power series reflect the effects of the weather conditions that occurred during the observation period and therefore contain part of the corresponding meteorological information. However, this indirect representation may be insufficient when future weather conditions differ substantially from historical patterns, particularly during rapidly changing or extreme weather events. Future research will incorporate explicit meteorological variables and numerical weather prediction information, including wind speed, solar irradiance, and temperature, into the forecasting framework. The effects of extreme weather conditions on renewable power forecasting and the resulting SES planning decisions will also be examined.

Data availability statement

The original contributions presented in the study are included in the article/supplementary material, further inquiries can be directed to the corresponding author.

Author contributions

ZY: Data curation, Formal Analysis, Conceptualization, Writing – original draft. WX: Project administration, Methodology, Investigation, Writing – original draft. YZ: Resources, Project administration, Writing – original draft, Methodology. XD: Supervision, Writing – original draft, Visualization. XZ: Writing – original draft, Visualization, Supervision, Validation.

Funding

The author(s) declared that financial support was not received for this work and/or its publication.

Conflict of interest

Authors ZY, WX, YZ, XD, and XZ were employed by Henan Jiuyu Longyuan Energy Service Co., Ltd.

Generative AI statement

The author(s) declared that generative AI was not used in the creation of this manuscript.

Any alternative text (alt text) provided alongside figures in this article has been generated by Frontiers with the support of artificial intelligence and reasonable efforts have been made to ensure accuracy, including review by the authors wherever possible. If you identify any issues, please contact us.

Publisher's note

All claims expressed in this article are solely those of the authors and do not necessarily represent those of their affiliated organizations, or those of the publisher, the editors and the reviewers. Any product that may be evaluated in this article, or claim that may be made by its manufacturer, is not guaranteed or endorsed by the publisher.

References

Bala Duranay, Z. (2023). Extreme learning machine-based power forecasting in photovoltaic systems. *IEEE Access* 11, 128923–128931. doi: 10.1109/access.2023.3333667

Chen, X., Ge, X., Sun, R., Wang, F., and Mi, Z. (2024). A SVM based demand response capacity prediction model considering internal factors under composite program. *Energy* 300, 131460. doi: 10.1016/j.energy.2024.131460

Dokur, E., Erdogan, N., and Yuzgec, U. (2025). Swarm intelligence-based multi-layer kernel Meta extreme learning machine for tidal current to power prediction. *Renew. Energy* 243, 122516. doi: 10.1016/j.renene.2025.122516

He, Y., and Zhang, Y. (2025). Optimal configuration of shared energy storage for multi-microgrid systems: integrating battery decommissioning value and renewable energy economic consumption. *Energy Convers. Manag.* 343, 120156. doi: 10.1016/j.enconman.2025.120156

Herwan Sulaiman, M., Mustaffa, Z., Jadin, M. S., and Saari, M. M. (2025). Hierarchical power output prediction for floating photovoltaic systems. *Energy* 323, 135883. doi: 10.1016/j.energy.2025.135883

Hou, Z., Zhang, Y., Cheng, X., and Ye, X. (2025). Photovoltaic power forecasting based on variational mode decomposition and long short-term memory neural network. *Energies* 18 (13), 3572. doi: 10.3390/en18133572

Huang, Y. (2026). Spatio-temporal prediction of wind power production-based on empirical data in Great Britain from 2021 to 2023. *Int. J. Electr. Power and Energy Syst.* 176, 111749. doi: 10.1016/j.ijepes.2026.111749

Jia, L., Wang, G., and Pang, X. (2025). A short-term wind power forecasting approach based on model configuration optimization *via* Prequential-Cross cooperative validation estimation. *Sustainability*, 17(22): 1–29. doi: 10.3390/su17229929

Kang, K., Jia, H., Hui, H., and Liu, D. (2025). Two-stage optimization configuration of shared energy storage for multi-distributed photovoltaic clusters in rural distribution networks considering self-consumption and self-sufficiency. *Appl. Energy* 394, 126174. doi: 10.1016/j.apenergy.2025.126174

Li, M., Li, F., Qiu, J., Zhou, H., Wang, H., Lu, H., et al. (2024a). Multi-objective optimization of non-fossil energy structure in China towards the carbon peaking and carbon neutrality goals. *Energy* 312, 133643. doi: 10.1016/j.energy.2024.133643

Li, J., Liu, Da, Jiang, S., and Wu, L. (2024b). Optimal configuration of shared energy storage system in microgrid cluster: economic analysis and planning for hybrid self-built and leased modes. *J. Energy Storage* 104, 114624. doi: 10.1016/j.est.2024.114624

Li, C., Liu, Y., Li, J., Liu, H., Zhao, Z., Zhou, H., et al. (2024c). Research on the optimal configuration method of shared energy storage basing on cooperative game in wind farms. *Energy Rep.* 12, 3700–3710. doi: 10.1016/j.egyr.2024.09.053

Li, M., Wan, J., Shi, J., Yao, K., and Ren, G. (2026). A wind power prediction method fusing deep learning with rolling adaptive successive variational mode decomposition. *Renew. Energy* 261, 125223. doi: 10.1016/j.renene.2026.125223

Lin, F., Zhang, H., Zhao, H., Huo, W., and Wang, J. (2025). Short-term probabilistic forecasting for regional PV power based on convolutional graph neural network and parameter transferring. *IEEE Trans. Power Syst.* 40 (3), 2724–2736. doi: 10.1109/tpwrs.2024.3503288

Liu, J., and Song, Y. (2025). Multi-objective configuration optimization model of shared energy storage on the power side. *J. Energy Storage* 114, 115706. doi: 10.1016/j.est.2025.115706

Liu, X., and Zhang, Q. (2024). Combining seasonal and trend decomposition using LOESS with a gated recurrent unit for climate time series forecasting. *IEEE Access* 12, 85275–85290. doi: 10.1109/access.2024.3415349

Oruç, S., Ali Hınıs, M., and Tuğrul, T. (2026). Forecasting photovoltaic power in high-latitude regions *via* support vector machine optimized by meta-heuristics. *Sci. Rep.* 16 (1), 3438. doi: 10.1038/s41598-025-33415-7

Patel, S., Ghosh, A., and Ray, P. K. (2025). Power management and control of a DC microgrid with hybrid energy storage systems using hybrid ANN-Based model predictive control. *J. Energy Storage* 105, 114726. doi: 10.1016/j.est.2024.114726

Peng, T., Son, S., Suo, L., Wang, Y., Nazir, M. S., and Zhang, C. (2024). Research and application of a novel graph convolutional RVFL and evolutionary equilibrium optimizer algorithm considering spatial factors in ultra-short-term solar power prediction. *Energy* 308, 132928. doi: 10.1016/j.energy.2024.132928

Tong, S., Jiang, A., Luo, J., Hu, H., An, Z., and Zhang, S. (2026). Dual-channel feature extraction and weather-guided two-stage clustering for short-term photovoltaic power prediction. *Renew. Energy* 257, 124764. doi: 10.1016/j.renene.2025.124764

Wang, C., Ma, Y., Xie, J., and Ouyang, Q. (2025). Multi-objective energy dispatch with deep reinforcement learning for wind–solar–thermal–storage hybrid systems. *J. Energy Storage* 105, 114635. doi: 10.1016/j.est.2024.114635

Wang, W., Liang, Y., Ci, T., and Kong, Z. (2026). Operational optimization of shared energy storage configuration in village-level distribution networks considering self-balancing capability. *J. Energy Storage* 141, 119385. doi: 10.1016/j.est.2025.119385

Wen, J., and Xie, X. (2026). Short-term load forecasting based on the improved bi-directional long short-term memory model. *Int. J. Electr. Power and Energy Syst.* 177, 111789.

Xuejun, Li, Wang, L., and Dong, Yu (2025). Intelligent planning and scheduling strategies for low-carbon distribution networks under high proportions of renewable energy integration. *Int. J. Low-carbon Technol.* 20, 129–135.

Yang, H., Tang, J., Wu, S., Yin, J., and Liu, B. (2025). Wind power data cleaning using RANSAC-Based polynomial and linear regression with adaptive threshold. *Sci. Reports* 15 (1), 5105. doi: 10.1038/s41598-025-89177-9

Yuan, H., Yue, W., Dou, C., Hancke, G. P., Zhang, Z., Wei, X., et al. (2026). Aggregated distributed photovoltaics-based active fast power-frequency regulation in the new power system. *IEEE Trans. Sustain. Energy* 17 (2), 1728–1740. doi: 10.1109/tste.2025.3629695

Zhang, Y., Wang, H., Wang, J., Cheng, X., Wang, T., and Zhao, Z. (2024a). Ensemble optimization approach based on hybrid mode decomposition and intelligent technology for wind power prediction system. *Energy* 292, 130492. doi: 10.1016/j.energy.2024.130492

Zhang, Y., Li, T., Ma, T., Yang, D., and Sun, X. (2024b). Short-term photovoltaic power prediction based on extreme learning machine with improved dung beetle optimization algorithm. *Energies* 17 (4), 960. doi: 10.3390/en17040960

Zhao, H., Zhang, Y., Huo, W., Lin, F., and Wang, J. (2026). A two-stage ensemble learning framework for short-term nonparametric probabilistic photovoltaic power forecasting integrating multi-source numerical weather predictions. *IEEE Trans. Power Syst.* 41 (2), 1231–1245. doi: 10.1109/tpwrs.2025.3613446

Zhou, J., Jia, R., Ren, J., Zhao, R., Wang, Y., and Wu, Y. (2025). Digital intelligence-driven synergistic optimization of capacity configuration for wind-solar-hydrogen multi-energy systems integrated with shared energy storage. *Energy* 341, 139497. doi: 10.1016/j.energy.2025.139497

Zhu, S., Ma, H., Chen, L., Wang, B., Wang, H., Li, X., et al. (2024). Short-term load forecasting of an integrated energy system based on STL-CPLE with multitask learning. *Prot. Control Mod. Power Syst.* 9 (6), 71–92. doi: 10.23919/pcmp.2023.000101

Glossary

a_k	The fuel cost coefficients
$P_{pv}^{cur}(t)$	Curtailed solar power
b	Bias term
$P_{wt}(t)$	The forecasted wind power
b_k	The fuel cost coefficients
$P_{pv}(t)$	The forecasted solar power
c_k	The fuel cost coefficients
$P_{load}(t)$	The load demand
$\vec{C}_{\max}$	Upper bound of the search space
$P_k^{\min}$	The minimum stable output
$\vec{C}_{\min}$	Low bound of the search space
$P_k^{\max}$	The maximum stable output
$\vec{C}_{eq}$	The concentration of guide particles
$\vec{r}_i$	Random vector
C_{ess}^{inv}	The investment cost of energy storage
$R_k^{\uparrow}$	The maximum ramp-up rates
C_{ess}^{om}	Operation and maintenance cost
$R_k^{\downarrow}$	The maximum ramp-down rates
C_{gen}	The total generation cost
$T_{k,t}^{\text{off}}$	The continuous downtime
$C_{k,t}^{\text{gen}}$	The fuel cost
α	Quadratic penalty operator
C_{cur}	The penalty cost
α_i	Lagrange multipliers
$C_{k,t}^{\text{su}}$	The start-up and shut-down cost
α_i^*	Lagrange multipliers
C_k^{hot}	The hot start cost
λ	Lagrange multiplier
C_k^{cold}	The cold start cost
$\vec{\lambda}$	Random vector
d	Dimensionality of the input space
λ_{ess}^{P}	The unit power construction cost
E_{ess}^{inv}	The investment construction capacity
λ_{ess}^{E}	The unit capacity construction cost
$f(t)$	Original signal
λ_{ess}^{om}	The unit operational and maintenance cost
$\vec{F}$	Exponential term
λ_{cur}	The unit punishment cost
$\vec{G}$	Randomly selected solution
u_k	Modal component
$G\vec{C}P$	The control parameter
ω_k	The center frequency
$Iter$	The number of current iterations
ω	Weight vector
j	Imaginary unit
τ	Step size parameter
Max_iter	The maximum number of iterations
δ	Noise discrimination accuracy
N	Population particle quantity
ε	Convergence progress
P_{ess}^{inv}	The investment construction power
$\mathbb{R}$	The real number field
$P_{ess}^{ch}(t)$	The charging power
ϑ	The width of insensitive loss zone
$P_{ess}^{dch}(t)$	The discharging power
$P_{wt}^{cur}(t)$	Curtailed wind power
v	The width of the RBF kernel